On Accuracy of Simple FDTD Models for the Simulation of Human Body Path Loss

Sergey N. Makarov, Umair I. Khan, Md. Monirul Islam, Reinhold Ludwig, Kaveh Pahlavan
Electrical and Computer Engineering
Worcester Polytechnic Institute
Worcester, MA, USA
{makarov, uikhan, monir, ludwig, kaveh}@wpi.edu

Abstract - **This paper compares a basic, MATLAB coded, time-domain FDTD formulation for the path loss around the human body with accurate FEM modeling in Ansoft HFSS (ANSYS). We show that the time domain FDTD analysis yields comparable results even though it uses a homogeneous body model and simple boundary conditions. Reasons for this important observation are investigated. The present study only considers the exterior TX and RX antennas, which are located close to the body. A more detailed FDTD simulation of on-body antennas [1] is currently underway.**

I. INTRODUCTION AND RELATED WORK

In the past decade miniaturization and declining costs of semiconductor devices have allowed design of small, low-cost computing and wireless communication devices. These are used as sensors in a variety of popular wireless networking applications and this trend is expected to continue in the next two decades. One of the most promising areas of economic growth associated with this industry is being termed *wireless Body Area Networks* (BAN) or *Body Sensor Networks* (BSN). These networks are expected to connect wearable and implantable sensory nodes together and with the Internet as part of the emerging "Internet of Things" These networks will support numerous applications ranging from traditional externally mounted temperature meters or implanted pace makers to emerging blood pressure sensors, eye pressure sensors for glaucoma, and smart pills for precision drug delivery. A number of technical challenges regarding size and cost, energy requirements, and wireless communication technology are under investigation and at the core of these investigations is the importance of understanding radio propagation in and around the human body.

In January 2003, the Federal Communication Commission (FCC) defined a standard for medical implant communication, allowing two-way communication between implants in a frequency band at 402-405 MHz with a maximum signal bandwidth of 300 kHz. This band is called the *Medical Implant Communication Services* (MICS) band. The IEEE 802.15.6 Working Group was then formed to address standardization of these emerging technologies. As part of its deliberations, the IEEE 802.15.6 Working Group defines the technologies and models for characteristics of the medium for wearable and implanted sensor networks.

The human body is not an ideal medium for RF wave transmission. It is partially conductive and consists of materials of different dielectric constants, thickness, and characteristic impedance. Therefore, depending on the frequency of operation, the human body can exhibit high power absorption, central frequency shift, and radiation pattern disruption. The absorption effects vary in magnitude with both frequency of the applied field and the characteristics of the tissue. The shadowing should be considered for stationary and non-stationary position of body. Because of multipath reflections, the channel response of a BAN channel resembles a series of pulses. In practice the number of pulses that can be distinguished is very large and depends on the time resolution of the measurement system. The power delay profile of the channel is an average power of the signal as a function of the delay with respect to the first arrival path.

II. CIRCUIT MODEL OF PATH LOSS

When time-domain and frequency-domain models are to be compared with each other, adequate source modeling is a critical issue. Figure 1 shows the simple TX/RX model used in this study to estimate the path loss and antenna-to-antenna transfer function for FDTD and FEM models. The generator is an ideal voltage source, V_g, in series with a generator resistance, R_g, connected to a TX antenna. The receiver is an RX antenna connected to a load resistance, R_L. All voltages and currents in Figure 1 are either real quantities (time domain FDTD) or complex phasors (frequency-domain FEM). Of primary interest is the received load voltage, V_L, as a function of the generator voltage V_G. This approach gives us the voltage transfer function T_V in phasor form

$$T_V = \frac{V_L}{V_g} \tag{1a}$$

The voltage transfer function depends on the values of the series resistors, the antenna impedances, and the associated path loss. Alternatively, one may be interested in the power transfer function, T_P which in phasor form is given by

$$T_P = \frac{P_L}{P_g} = \frac{|V_L|^2/(2R_L)}{|V_g I_g^*|/2} \tag{1b}$$

The transfer functions are determined using the simulation data as described below.
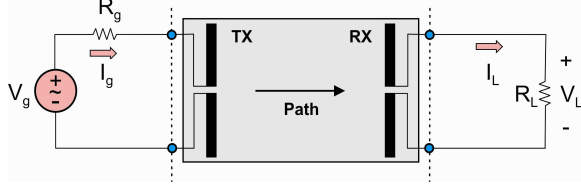

Figure 1 Circuit model of antenna-to-antenna TX/RX link.

III. TRANSFER FUNCTIONS IN FREQUENCY DOMAIN

When using the FDTD simulations, both transfer functions in Equations (1) are found directly in the time domain using the proper excitation models [2],[3]. This method is explained in Section 3 below. For the FEM frequency-domain Ansoft HFSS analysis we use a lumped-circuit approach as shown in Figure 2. For a system with two lumped ports (TX and RX antennas), this approach employs the impedance matrix $\hat{Z}$ of size 2×2, which is readily available as "solution data" in HFSS for a particular frequency. The impedance matrix is invariant to specified port impedances. The TX-RX antenna network shown in Figure 1 can thus be replaced by an equivalent two-port microwave network described by the impedance matrix $\hat{Z}$ depicted in Figure 2b [4], [5]

$$\hat{Z} = \begin{bmatrix} Z_{11} & Z_{12} \\ Z_{21} & Z_{22} \end{bmatrix} \tag{2}$$
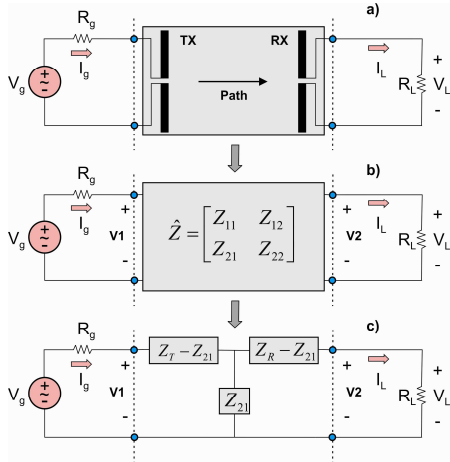

Figure 2 Network transformations of the antenna-to-antenna link; a) original TX/RX network; b) microwave impedance matrix approach; and c) equivalent T-network of lumped impedances.

The impedance approach is more appealing for this problem than the scattering S- matrix approach, since the S parameters always require an extra transmission line section at each port. Furthermore, the impedance approach explicitly relates the antenna link to the circuit parameters, and thus allows us to directly employ the well-known analytical results for small dipole and loop antennas. For reciprocal antennas, the mutual impedances are identical, i.e. $Z_{12} = Z_{21}$. When the antennas are located far way from each other, the self-impedances Z_{11}, Z_{22} are not affected by the presence of the second antenna as a scatterer, and are reduced exact antenna impedances in free space, i.e.

$$Z_{11} = Z_T, \ Z_{22} = Z_R \tag{3}$$

Thus, the two-port network in Figure 2b, with the impedance matrix given by Equation (1), is replaced by an equivalent T-network (a Π-equivalent network is also possible, but it is not considered). The resulting circuit is depicted in Figure 2c. The solution for the receiver voltage then becomes a straight-forward circuit analysis with the final result

$$V_L(\omega) = \frac{R_L Z_{21}}{(Z_R + R_L)(Z_T + R_g) - Z_{21}Z_{21}} V_g(\omega) \tag{4}$$

for the voltage transfer function known as the forward voltage gain. An equation for the power transfer could be obtained in a similar way.

IV. TRANSFER FUNCTIONS IN TIME DOMAIN

The lumped port model in FDTD follows reference [6] and is shown in Figure 3. It occupies one unit cell. The generator circuit includes the open gap antenna feed with the electric field $E_z(t, x_e, y_e, z_e)$, which is updated based on the Maxwell equations in free space. We apply KVL to loop 1 as indicated in Figure 3. This yield:

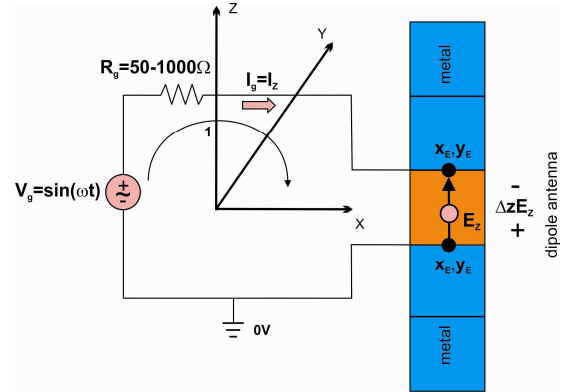$$-V_g(t) + R_g I_g(t) - \Delta z E_z(t, x_e, y_e, z_e) = 0 \tag{5}$$

Figure 3 FDTD port model corresponding to the excitation source in Figure 1.

Solving Equation (5) for the current results in

$$I_g(t) = \frac{1}{R_g} V_g(t) + \frac{\Delta z}{R_g} E_z(t, x_e, y_e, z_e) \tag{6}$$

The FDTD version of Equation (6) becomes

$$I_{z\,k,m,p+1/2}^{n} = \frac{\Delta z}{R_g} E_{z\,k,m,p+1/2}^{n} + \frac{1}{R_G} V^{n} \qquad (7)$$

where k, m, p are grid-related integers and n is discrete time. According to reference [6], this is the "semi-implicit formulation" for the conduction current in the sense that this current relies in part upon the updated electric field to be determined as a result of the time stepping; and it does not result in a system of simultaneous equations. This yields a numerically stable algorithm for arbitrary positive resistance values. Using Ampere's law with an impressed current source from Equation (7) one has the fully explicit formulation for the source

$$E_z^{n+1} = e_{S1} E_z^{n} + e_{S2}\Delta_x H_y^{n+1/2} - e_{S2}\Delta_y H_x^{n+1/2} - e_{S3}\frac{1}{2}\left(V^{n+1} + V^{n}\right) \qquad (8)$$

where

$$\sigma = \frac{\Delta z}{R_g \Delta x \Delta y} = \frac{1}{R_g \Delta}, \quad e_{S1} = \frac{1 - \frac{\Delta t \sigma}{2\varepsilon_{k,m}}}{1 + \frac{\Delta t \sigma}{2\varepsilon_{k,m}}}, \quad e_{S2} = \frac{\frac{\Delta t}{\varepsilon_{k,m}\Delta}}{1 + \frac{\Delta t \sigma}{2\varepsilon_{k,m}}}, \quad e_{S3} = \frac{\frac{\Delta t \sigma}{\varepsilon_{k,m}\Delta}}{1 + \frac{\Delta t \sigma}{2\varepsilon_{k,m}}}$$

$$(9)$$

with $\Delta = \Delta x = \Delta y = \Delta z$ being the unit cell size. Equations (7) gives us the generator current in the time domain, see

Figure 1. For the receiver in Figure 1, Equations (7) – (9) again apply, but with the voltage source set equal to zero. The receiver voltage is thus given by

$$V_L(t) = R_L I_L(t) \qquad (10)$$

The transmitted and received powers are found in the same fashion.

V. COMPARISON BETWEEN FDTD AND FEM FOR ANTENNA TO ANTENNA LINK IN FREE SPACE

We consider two electrically small dipole antennas at 402 MHz, shown in Figure 4. Both antennas have a total length of 11.25 cm, which is considerably less than the half wavelength of 37.3cm. Therefore, both of them have a large capacitive reactance and a small radiation resistance. The antennas are assumed to consist of thin metal strips with width of 1.25cm. The antenna separation distance (from center to center) is 41.3cm, which implies a near-field link. The FDTD method uses the Yee second- order differences on a staggered grid; it is programmed according to Ref. [1].
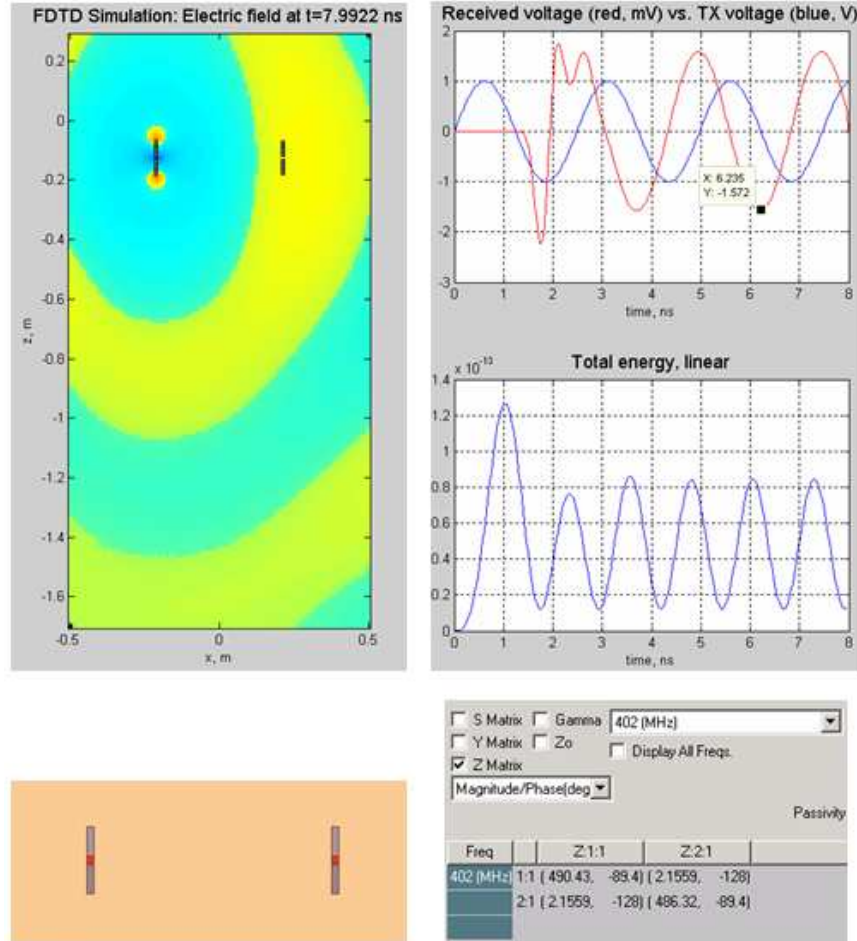

Figure 4 Top: FDTD simulations of the dipole-to-dipole link in free space; Bottom: corresponding Ansoft HFSS simulations with resulting impedance matrix. The transition region of the FDTD solution is clearly seen; it averages about 4 ns.

For simplicity, we only use the first-order Mur's ABCs [7] augmented with the superabsorption update [8] for the magnetic field. The FDTD domain shown in Figure 4-top is larger than required; it is set up for the prospective human body modeling. Figure 4-top also shows the received voltage as a function of time versus the transmitted voltage. The entire FDTD algorithm is implemented in MATLAB. The total energy plot in Figure 4 indicates a large reactive energy component that is typical for the near field of non-resonant antennas. The equivalent Ansoft HFSS simulation is performed using a perfectly matched layer (PML) absorbing boundary condition and a large number of tetrahedra in the FEM mesh (about 50,000). We calculate the receiver voltage in Ansoft using Equation (4) and the receiver voltage in FDTD using Equation (10).

Table 1 provides the received voltage amplitude for different values of generator/load resistances. We assume $R_g = R_L$. The source has the amplitude of 1V in all cases. One can see that the difference between the two approaches does not exceed 9%. This is generally of sufficient accuracy for path loss modeling.

TABLE I. RECEIVED VOLTAGE AMPLITUDE FOR DIFFERENT VALUES OF $R_g = R_L$. THE SOURCE HAS AN AMPLITUDE OF 1 V.

$R_g = R_L$	Ansoft HFSS data for the received voltage amplitude	FDTD data for the received voltage amplitude
50Ω	0.44mV	0.45mV
1000Ω	1.57mV	1.72mV

VI. COMPARISON BETWEENT FDTD AND FEM FOR HUMAN BODY MODELING

The Ansoft human body model has frequently been used in FEM simulations. This highly accurate model includes more than 20 internal meshes separately modeling heart, kidney, liver, blood, etc. After six iteration passes, we ended up with meshes on the order of 1,000,000 tetrahedra with execution times on the order of 24 hours. The corresponding geometry is shown in Figure 5. We consider the same two electrically small dipole antennas at 402 MHz. The antenna shift in Figure 5 along the z-axis in local Ansoft HFSS coordinates is -130.5mm, -190.5mm, and -390.5mm. The antenna separation distance is the same as before.

We have exported the identical human body volume from Ansoft to MATLAB's FDTD mesh. In the FDTD model, we then assigned the average relative dielectric constant of 50 and the average body conductivity of 0.5S/m to the body volume with any large conductivity. The lungs, however, remain as air. All antenna parameters stay the same. The execution times in MATLAB are about 7 minutes for a FDTD mesh of about 800,000 individual bricks.

Table 2 reports the received voltage amplitude obtained using the two methods for different values of $R_g = R_L$, and different antenna positions. The source always has the amplitude of 1V. One can see that the agreement between the two data sets is excellent; the error does not exceed 12% in every case. Such an observation is important since it allows us to use the much faster (by the factor of ~100) FDTD model for obtaining accurate results.

TABLE II. RECEIVED VOLTAGE AMPLITUDE FOR DIFFERENT VALUES OF $R_g = R_L$ AND DIFFERENT ANTENNA POSITIONS. THE SOURCE HAS AN AMPLITUDE OF 1 V.

$R_g = R_L$	Antenna shift in the vertical direction	Ansoft HFSS data for the received voltage amplitude	FDTD data for the received voltage amplitude
1000Ω	-130.5mm	0.37mV	0.38mV
50Ω	-130.5mm	0.10mV	0.12mV
1000Ω	-190.5mm	0.28mV	0.29mV
50Ω	-190.5mm	0.077mV	0.86mV
1000Ω	-390.5mm	0.025mV	0.024mV
50Ω	-390.5mm	0.007mV	Noise floor

VII. DISCUSSION

Why does the coarse homogeneous body model in FDTD operate almost identically to the accurate FEM model? We believe that the major reason lies in the reflection of the RF signal directly from the body surface and its further diffraction around the body. When the two antennas are located outside the body, the near-field diffraction path is the dominant path of the wireless link.

Furthermore, the EM field that enters the body is very weak due to the large impedance difference. It undergoes path loss within the body and an additional reflection loss before it leaves the

body. Consequently, its contribution is insignificant, at least in this present study.
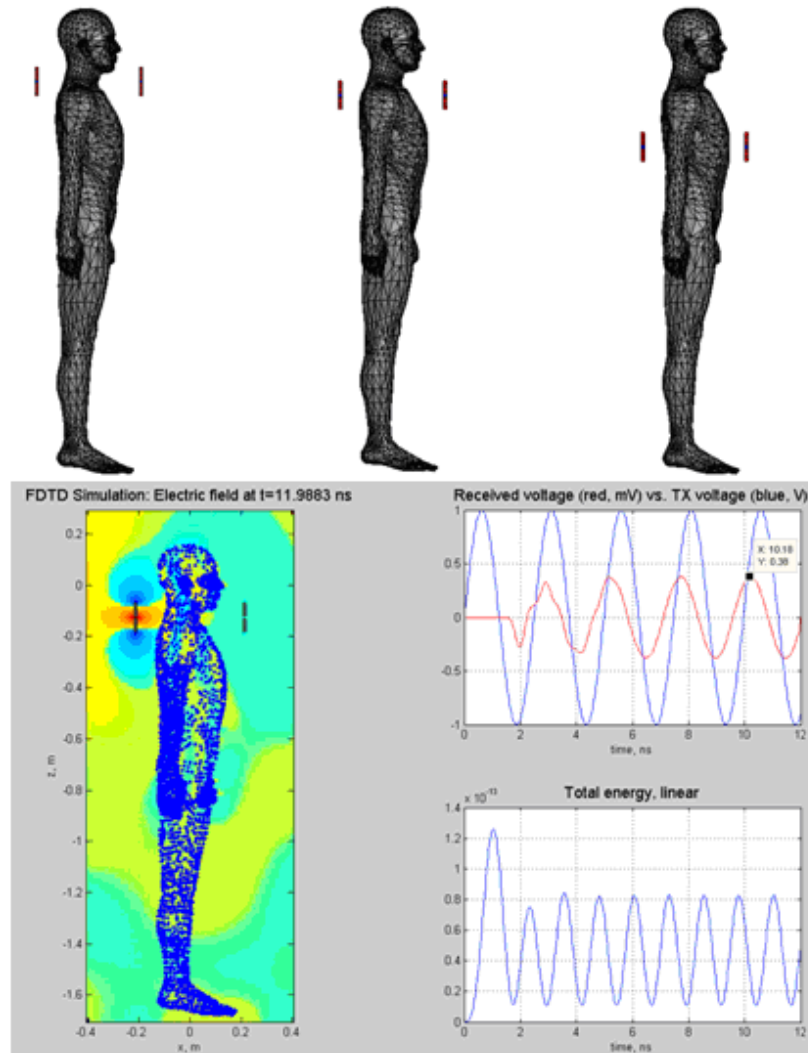

Figure 5 Antenna locations positioned around the human body. The antenna separation distance is fixed at 41.3cm. Top: FEM Ansoft mesh; Bottom: FDTD mesh; simulation results corresponding to the first case, and electric field distributions. The electric field is scaled by a power of 0.2 in order to accentuate the extremely small field strength levels seen in the figure.

VIII. CONCLUSIONS

In this paper we have compared a basic time-domain FDTD simulation for the path loss around the human body in MATLAB with accurate FEM modeling of the human body in Ansoft HFSS (ANSYS). We have shown that the time domain FDTD analysis yields comparable results even when it uses a homogeneous body model and simple boundary conditions. The reason for this important observation is that the diffraction path around the human body is the major propagation path between transmitter and receiver. This study only considers the exterior TX and RX antennas, which are located close to the body. Two key questions need to be addressed as we continue this study:

1. How close to the body surface can the antennas be positioned in order for this observation to remain true?
2. What happens for two on-body antennas? Is the diffraction (surface wave) path still dominant?

[1] H. Terchoune, D. Lautru, A. Gati, A. Cortel Carrasco,M. Faï Wong, J. Wiart, and V. F. Hanna, "On-body radio channel modeling for different human body models using FDTD techniques," vol. 51, no 10, Oct. 2009, pp. 2498-2501.

[2]   A. Taflove, *Computational Electrodynamics, The Finite Difference Time Domain Approach*, Artech House, Norwood, MA, 1995.

[3]   A. Bondeson, T. Rylander and P. Ingelström, *Computational Electromagnetics*, Springer, New York, 2005, Series: Texts in Applied Mathematics, Vol. 51. pp. 58-86.

[4]   C. A. Balanis, *Antenna Theory*, Wiley, New York, 2005, 3rd ed, pp. 468-470.

[5]   D. M. Pozar, *Microwave Engineering*, Wiley, New York, 2005, 3rd ed.

[6]   M. Piket-May, A. Taflove, and J. Baron, "FD-TD modeling of digital signal propagation in 3-D circuits with passive and active loads," *IEEE Trans. Microwave Theory and Techniques*, vol. 42, no. 8, Aug. 1994, pp. 1514 - 1523.

[7]   G. Mur, "Absorbing boundary conditions for the finite-difference approximation of the time-domain electromagnetic field equations," *IEEE Trans. Electromagn. Compat.*, vol. EMC-23, no. 4, pp. 377-382, Nov. 1981.

[8]   K. K. Mei and J. Fang, "Superabsorption – a method to improve absorbing boundary conditions," *IEEE Trans. Antennas and Propagation*, vol. 40, no. 9, Sep. 1992, pp. 1001- 1010.

[9]   J.-P. Bérenger, "A perfectly matched layer for the absorption of electromagnetic waves," *J. Comput. Phys.*, vol. 114, pp. 185–200, Oct. 1994.

[10]   D. S. Katz, E. T. Thiele, and A. Taflove, "Validation and extension to three dimensions of the Berenger PML absorbing boundary condition for FD-TD meshes," *IEEE Microwave and Guided Wave Letters*, vol. 4, no 8, Aug. 1994, pp. 268-270.